THE JOURNAL OF BIOLOGICAL CHEMISTRY
Vol. 269, No. 50, Issue of December 16, pp. 31785–31792, 1994
Printed in U.S.A.

Solution Structure of Taxotere-induced Microtubules to 3-nm Resolution

THE CHANGE IN PROTOFILAMENT NUMBER IS LINKED TO THE BINDING OF THE TAXOL SIDE CHAIN*

(Received for publication, July 18, 1994, and in revised form, September 12, 1994)

Jose M. Andreu‡§, J. Fernando Díaz‡, Rosario Gil‡, Jose M. de Pereda‡, Mario García de Lacoba‡, Vincent Peyrot¶, Claudette Briand¶, Elizabeth Towns-Andrews‖, and Joan Bordas‖

From the ‡Centro de Investigaciones Biológicas, Consejo Superior de Investigaciones Científicas, Velazquez 144, 28006 Madrid, Spain, the ¶GRIPP, Faculté de Pharmacie, 27 Boulevard Jean Moulin, 13385 Marseille Cedex 5, France, and the ‖Daresbury Laboratory, Warrington WA4 4AD, United Kingdom

The synchrotron x-ray solution scattering profiles of microtubules assembled from purified GDP- or GTP-tubulin with the antitumor drug docetaxel (Taxotere®) are consistent with identical non-globular α and β-tubulin monomers ordered within the known surface lattice of microtubules, with a center to center lateral spacing of 5.7 ± 0.1 nm. The higher angle part of the scattering profile, and therefore the substructure of the microtubule wall is identical in Taxotere- and Taxol-induced microtubules, to the resolution of the measurements. However, Taxotere-induced microtubules have a mean diameter of 24.2 ± 0.4 nm, which is 1.12 ± 0.01 times larger than that of paclitaxel (Taxol®) induced microtubules. The population of Taxotere microtubules has on average 13.4 protofilaments, which is similar to control microtubules assembled with glycerol but is in marked contrast with Taxol-induced microtubules, which have on average 12 protofilaments under identical solution conditions. Model populations of Taxotere and Taxol microtubules with the distributions of protofilament numbers determined by electron microscopy reproduce the positions and approximate intensities of the experimental x-ray scattering data. Comparison of the structures and activities of both taxoids strongly suggests that the change of the more frequent lateral bond angle between tubulin molecules from 152.3° (13-protofilament microtubules) to 150° (12-protofilament microtubules) is linked to the binding of the side chain of Taxol. Optimal microtubule formation is obtained with unitary Taxotere to tubulin heterodimer ratio; however, ligand molecules in excess over tubulin dimers cause a loss of cylindrical scattering features, consistent with microtubule opening. The results are compatible with the observed biochemical and thermodynamic properties of this ligand-induced microtubule assembly system and also with the simple working hypothesis that taxoids would bind between adjacent microtubule protofilaments.

Microtubules are dynamic components of the cytoskeleton essential in cellular organization and main constituents of the mitotic spindle. They are formed by reversible assembly of the αβ-tubulin dimer into long hollow cylinders, typically made of 13 protofilaments, to whose outer surface microtubule-associated proteins and cytoplasmic motors bind. Tubulin is the target of mitosis-arresting drugs, many of which inhibit its correct assembly (1, 2). Taxol[1] is an antitumor compound extracted in small amounts from the non-renewable bark of the Pacific yew (3–6), which is now clinically available as an anticancer drug. Taxol is effective against a number of advanced tumors, including recurrent advanced ovarian cancer and breast cancer (7, 8). Taxol has the unique property of inducing microtubule assembly *in vitro* and in cells (9–11) and appears to block cell division by kinetically stabilizing spindle microtubules (12). The scarcity of Taxol has stimulated the search of alternative sources. Taxol is also obtained from cell cultures of *Taxus* (13) or of *Taxomyces*, a fungal endophyte of the Pacific yew (14). The total synthesis of Taxol has recently been achieved (15, 16).

10-Deacetyl baccatin III, isolated from the renewable needles of the yew, has been identified as the best precursor permitting the preparation of large amounts of semisynthetic Taxol (17) and of the new compound Taxotere (5, 18–20). Taxotere is more water-soluble and slightly more active than taxol (21–25), and it is in advanced clinical trials (26, 27). Taxol and Taxotere represent most significant landmarks among naturally occurring anticancer agents. Recent affinity photolabeling results with 3′-(*p*-azidobenzamido)taxol indicate that the activated side chain of the drug covalently binds to the N-terminal 31-amino acid fragment of β-tubulin (28), while the results with an ((azidophenyl)ureido)taxoid indicate predominant labeling of β- over α-tubulin (29). The taxoid-induced polymerization of purified tubulin constitutes a simplified model system of microtubule assembly and structure, which provides clues into the molecular mechanisms of action of these drugs. It was suggested that Taxol induces the lateral association of tubulin molecules in the microtubule wall (30). Taxoid-induced microtubule assembly has been shown to proceed even from inactive GDP-tubulin, and Taxotere apparently has twice the affinity of Taxol for the same binding site (31). The binding of both taxoids is thermodynamically linked to the assembly process, allowing it to proceed even in the cold, while binding to unassembled tubulin is practically undetectable (32). It has been proposed that the binding of the taxoids to oligomers (nucleation) and to microtubule ends (elongation) induces the switching of the

* This work was supported in part by Direccion General de Investigacion Científica y Técnica Grant PB92007, European Community Science Contract SC1-CT91-0658, and the Consejo Superior de Investigaciones Científicas program Acciones Especiales en Estructura y Función de Proteínas. Access to the Daresbury Laboratory Synchrotron Radiation Source was obtained through the European Community Large Scale Facilities Program. The costs of publication of this article were defrayed in part by the payment of page charges. This article must therefore be hereby marked "*advertisement*" in accordance with 18 U.S.C. Section 1734 solely to indicate this fact.

§ To whom correspondence should be addressed. Fax: 34-1-5627518.

[1] The names used are: Taxol® (Bristol-Myers Squibb) (paclitaxel), 4,10-acetoxy-2α-(benzoyloxy)-5β,20-epoxy-1,7β-dihydroxy-9-oxotax-11-en-13α-yl-(2*R*,3*S*)-3-[(phenylcarbonyl)amino]-2-hydroxy-3-phenylpropionate; Taxotere® (Rhône-Poulenc Rorer) (docetaxel), 4-acetoxy-2α-(benzoyloxy)-5β,20-epoxy-1,7β,10β-trihydroxy-9-oxotax-11-en-13α-yl-(2*R*,3*S*)-3-[(*tert*-butoxycarbonyl)amino]-2-hydroxy-3-phenylpropionate.

GDP-tubulin structure into the active conformation, and that these ligands might constitute molecular matchmakers that participate in the protein-protein interaction interfaces between the protofilaments of microtubules (32).

X-ray scattering methods are well suited to study different protein conformational and assembly states in solution. With high intensity synchrotron radiation, they give access to time-resolved low resolution structure (33–38). The low resolution structure of Taxol-induced microtubules has been shown to conform to the known microtubule surface lattice with non-globular tubulin monomers; however, microtubules assembled from purified tubulin and Taxol have on average only 12 protofilaments (37). Taxotere-induced microtubules have been examined in rigorous comparison with Taxol microtubules by synchrotron x-ray solution methods. The induction of structural differences in microtubules by the taxane side chain is evidenced. This gives further insight into microtubule structure and the mechanisms of taxoid interaction with microtubules.

MATERIALS AND METHODS

The preparation and taxoid-induced assembly of highly purified GDP- and GTP-tubulin and ligands were as described (31), except as otherwise indicated. X-ray scattering experiments were made at station 2.1 of the Daresbury Laboratory Synchrotron Radiation Source. Data acquisition and processing, computer modeling, and electron microscopy were as described previously (35, 37, 38). Absolute values of the scattering vector (defined as $S = 2(\sin\theta)/\lambda$, where 2θ is the angle of incident to scattered radiation and λ the x-ray wavelength) were calibrated in this work employing all the observable diffraction orders of the 67-nm repeat in wet rat tail collagen. A 3-m camera length was employed, effectively covering an S range from approximately 0.02 nm^{-1} to 0.33 nm^{-1}. The low resolution x-ray solution scattering patterns of microtubules were interpreted as described (37) by reference to their fiber diffraction, indexed on the basis of the well known helical surface lattice of microtubules (39).

RESULTS

Synchrotron X-ray Scattering of Taxotere-induced Microtubule Assembly—Time-resolved x-ray scattering of solutions of GDP-tubulin while undergoing assembly induced by equimolar Taxotere or Taxol, initiated by a slow temperature increase from 4 to 37 °C, showed that the increase in central scattering (due to the overall degree of polymerization) and the appearance of the microtubule features take place at lower temperatures for Taxotere than for Taxol (not shown). This indicated that Taxotere is a more powerful inducer of microtubules from GDP-tubulin than Taxol, which is fully consistent with the thermodynamics of this ligand-induced protein assembly system (32). Fig. 1 shows an experiment in which the Taxotere to tubulin heterodimer ratio was varied from nil to over 4-fold, assembly was initiated by a rapid temperature shift to 37 °C, and the time-independent x-ray scattering profiles of the end assembly products were measured to 3-nm resolution. In the absence of Taxotere there is no microtubule assembly (*curve 1*), though the steep central scattering indicates the formation of protein oligomers. The first, second, and third subsidiary maxima of the J_0 Bessel function correspond to the low resolution transform of the excess electron density of the cylindrical structures relative to the solvent. They grow with increasing drug concentration, are optimally formed at unitary Taxotere to tubulin dimer ratio (*curve 4*), and decay in excess ligand. The next three peaks at higher angles are sensitive to the microtubule surface lattice and to the shape of the monomer (37). They correspond to the equatorial J_n Bessel function and the helical J_3 and J_{n-3} Bessel functions, arising, respectively, from the electron density periodicity around a n protofilament microtubule and from the features in the direction the three-start and the n – 3-start helices in the microtubule lattice. The J_n maximum appears with increasing Taxotere, and its intensity

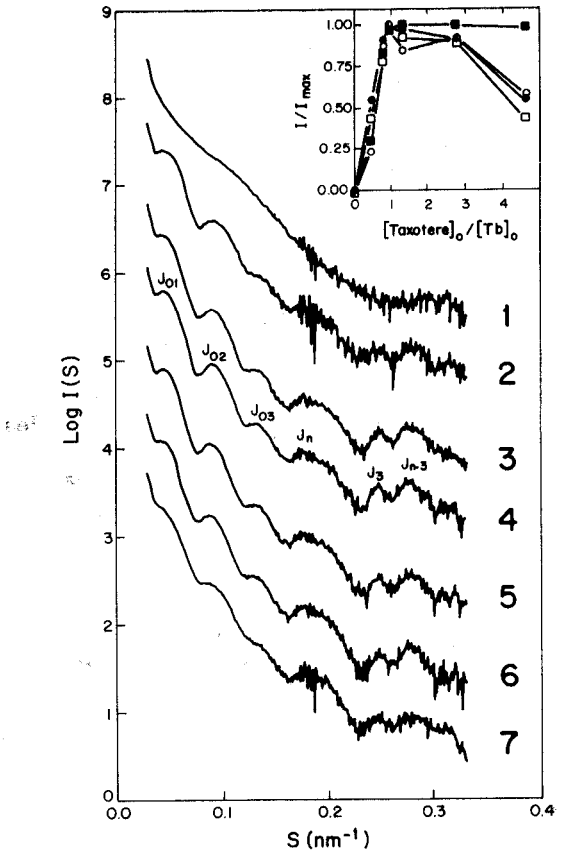

FIG. 1. **Stoichiometry of Taxotere-induced microtubule assembly.** GTP-tubulin was equilibrated in 10 mM phosphate, 6 mM $MgCl_2$, 1 mM GTP buffer, pH 6.7. The taxoid was added and the temperature was shifted from 4 °C to 37 °C. The final scattering profiles of the samples (assembled to invariant scattering features, after more than 25 min at 37 °C) are shown. *Curve 1*, 44 μM tubulin without Taxotere; *curve 2*, 44 μM tubulin + 20 μM Taxotere; *curve 3*, 56 μM tubulin + 43 μM Taxotere; *curve 4*, 44 μM tubulin + 40 μM Taxotere; *curve 5*, 56 μM tubulin + 73 μM Taxotere; *curve 6*, 56 μM tubulin + 154 μM Taxotere; *curve 7*, 56 μM tubulin + 255 μM Taxotere. All samples contained constant 2.5% (v/v) dimethyl sulfoxide. The *inset* shows the intensities of the peaks corresponding to the J_{02} (●), J_n (■), J_3 (○), and J_{n-3} (□) Bessel functions (which are labeled in the figure) as function of the molar ratio of total Taxotere to tubulin dimer in each solution.

reaches maximum value around one ligand molecule per tubulin heterodimer. In excess ligand the J_n intensity remains essentially invariant, in contrast to the decrease of the J_0 peak, as shown by Fig. 1 (*inset*). The J_3 and J_{n-3} peaks (whose intensities can be observed to decrease in opening microtubule models; not shown), appear to raise and decrease, similarly to those of the J_0, though the noise is larger at these higher angles. These results indicate that the microtubules loose cylindrical features in the presence of excess Taxotere. Sedimentation measurements have indicated that the amount of tubulin assembled is maximal at unitary ligand to protein ratio and remains essentially invariant at higher ratios (31). At the protein concentration of the x-ray experiment and up to a total ligand to protein mole ratio 3, the Taxotere bound was 1.01 ± 0.04 molecules ligand/GDP-tubulin dimer assembled, without any detectable trend (data from Ref. 31; Table I).

Fig. 2 compares the final x-ray scattering profiles of GTP- and GDP-tubulin assembled with Taxotere and Taxol. The four scattering curves 1, 2, 4, and 5 are related and correspond to a majority of microtubules in each sample. There is no significant difference between GTP and GDP. The Taxotere and Taxol microtubule scattering profiles are essentially identical at higher angles. However, at low angles it can be observed that the

TABLE I
Positions of the x-ray solution scattering maxima of microtubules

Composition of microtubules	Scattering maxima and position (S)						Mean helical radius[a]
	J_{01}	J_{02}	J_{03}	J_n	J_3	J_{n-3}	
			nm^{-1}				nm
Tubulin-Taxotere[b]	0.0496 ± 0.0007	0.092 ± 0.001	0.137 ± 0.001	0.193 ± 0.001	0.256 ± 0.001	0.285 ± 0.001	12.1 ± 0.2
Tubulin-Taxol[c]	0.0547 ± 0.0007	0.103 ± 0.001	0.154 ± 0.001	0.193 ± 0.001	0.256 ± 0.001	0.285 ± 0.001	10.8 ± 0.2
Tubulin-glycerol[d]	0.0497	0.091	0.138	0.192	0.263	0.288	12.1
Tubulin-Taxol[e]	0.0538	0.100	0.150	0.192	0.253	0.281	11.1
Tubulin-glycerol[e]	0.0496	0.092	0.137	0.190	0.25	0.281	12.1
Taxotere model mixture[f]	0.0497	0.092	0.136	0.192	0.250	0.283	12.1
Taxol model mixture[f]	0.0544	0.102	0.152	0.192	0.252	0.282	10.9

[a] Helical radii measured from the positions of the three first subsidiary maxima of the J_0 Bessel function (37, 38).
[b] Average and standard error of 14 different measurements of Taxotere microtubules.
[c] Average and standard error of 17 different measurements of taxol microtubules.
[d] Average of two measurements of glycerol microtubules.
[e] Data from previous measurements (37) with a slightly less accurate calibration of S values at high angles than in the present work, shown for comparison.
[f] Model microtubule populations 3 and 6 in Fig. 2.

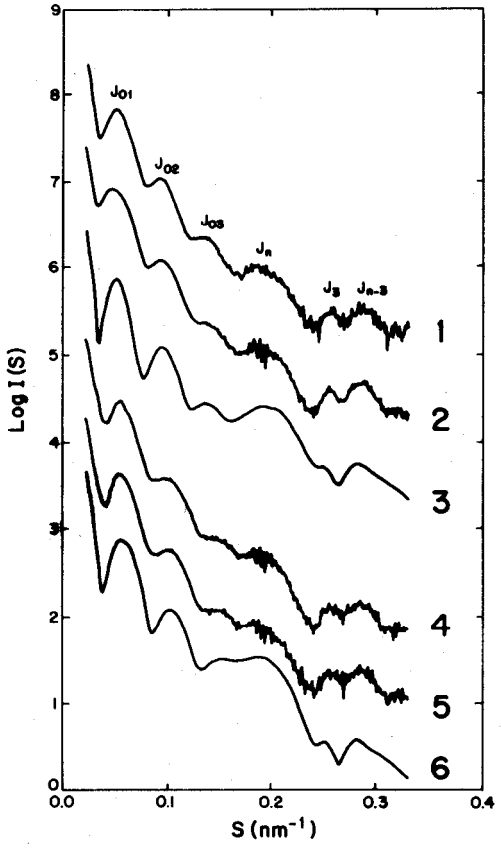

FIG. 2. **X-ray scattering profiles of Taxotere- and Taxol-induced microtubules.** GDP-tubulin in 10 mM phosphate, 1 mM EDTA, 7 mM $MgCl_2$, 1 mM GDP buffer, pH 6.7 (plus 1 mM GTP added to the GTP-tubulin samples; Ref. 31), was assembled with equimolar taxoid by a temperature shift to 37 °C. *Curve 1*, 93.5 μM GTP-tubulin-Taxotere; *curve 2*, 82.5 μM GDP-tubulin-Taxotere; *curve 3*, model microtubule population consisting of a mixture of microtubules of different protofilament numbers (Fig. 3), with the protofilament number distribution of Fig. 4*B*; *curve 4*, 140 μM GTP-tubulin-Taxol; *curve 5*, 78 μM GDP-tubulin-Taxol; *curve 6*, model microtubule population with the protofilament number distribution of Fig. 4*C*. The valleys between the J_0 peaks in both *curves 3* and *6* could be made to approach their corresponding data by inclusion of a 30% proportion of opened microtubules or 15% small tubulin oligomers (not shown).

position of the maxima of the J_0 peaks of Taxotere microtubules is shifted toward smaller scattering vector values with respect to Taxol microtubules.

Structure of Taxotere-induced Microtubules: Surface Lattice, Diameter, and Number of Protofilaments—The similarities and differences between Taxotere and Taxol microtubules can be better appreciated from their corrected intensity scattering profiles, shown by Fig. 3*A* (*solid* and *dashed line*, respectively). These profiles have been obtained by multiplying the x-ray scattering intensities by their corresponding S value, a procedure that allows better definition of the position of the maxima and a more direct comparison of solution scattering to fiber diffraction patterns. The position of each maxima are given in Table I, as well as its indexing based on the known helical surface lattice of microtubules (39), allowing for variable protofilament number. The structure of Taxotere-induced microtubules can be characterized from these data as follows. The J_n, J_3, and J_{n-3} region of the scattering profiles is identical for Taxotere and Taxol microtubules. Therefore, within the resolution and experimental error of present measurements, the microtubule surface lattice spacings and the tubulin monomer shape are indistinguishable in both types of microtubules, *i.e.* their wall substructure is most likely the same. However, the diameter of Taxotere microtubules, determined from the 1.12 ± 0.01 shorter S value of their J_0 maxima, is 24.2 ± 0.4 nm instead of 21.6 ± 0.4 nm (Taxol). Therefore, Taxotere microtubules have on average about one protofilament more than taxol microtubules. Since the majority of these taxol microtubules have 12 protofilaments (37), Taxotere-induced microtubules should typically have 13 protofilaments. Actually, the substitution of Taxotere for Taxol gives microtubules all of whose scattering maxima are back to positions very similar to those of control glycerol microtubules (Fig. 3*B* and Table I), which strongly suggests similar structures in Taxotere and glycerol microtubules.

Modeling and Electron Microscopy of Taxotere-induced Microtubules—The x-ray solution scattering profile of Taxotere-induced microtubules was modeled employing a simulation program based on Debye's formula (40), with microtubule lattices containing non-globular tubulin monomers (37). The superimposable high angle region of the scattering profiles of taxol and Taxotere microtubules was fitted first, for which a complete search of the limited possibilities of orientation of the monomer was made (similarly to the case of tubulin rings; Ref. 38). The monomers have to be obviously oriented at the same angles for both ligands, which were coincident with those of the previous modeling (37). The lateral spacing between the centers of mass of the monomers was varied, and the best fit to the J_n, J_3, and J_{n-3} peaks was obtained for a spacing of 5.7 ± 0.1 nm, as depicted by Fig. 3*C* (*inset*). The computed scattering profiles of three-start microtubule lattices (*solid line*) are compatible with the data, while two- and four-start models (*dashed* and *thin lines*) give small differences, which do not permit unequivocal distinction. Next, microtubule models with these characteristics and different number of protofilaments were

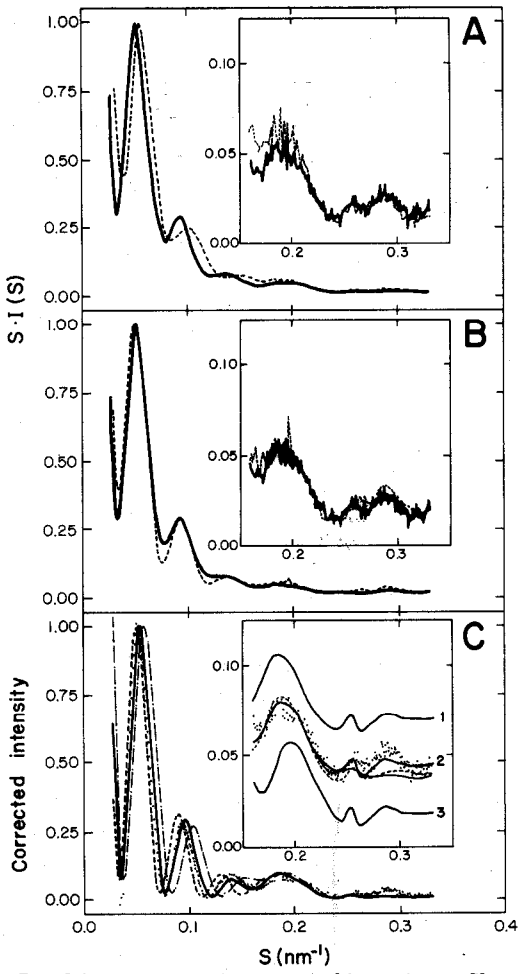

FIG. 3. *Panel A*, x-ray scattering corrected intensity profiles of microtubules assembled from GTP-tubulin-Taxotere (*solid line*), in comparison to GTP-tubulin-Taxol (*dashed line*). *Panel B*, GTP-tubulin-Taxotere microtubules (*solid line*) in comparison with microtubules assembled from GTP-tubulin with glycerol (*dashed line*). The *insets* are enlargements of the ordinate scale. For glycerol-induced assembly, tubulin was equilibrated in 10 mM sodium phosphate, 3.4 M glycerol, 1 mM EGTA, 1 mM GTP to which 6 mM $MgCl_2$ was added, final pH 6.5. *Panel C*, model calculations of the x-ray scattering profiles for 12 (*dot-dash line*), 13 (*continuous line*), and 14 protofilament (*dashed line*) microtubules, in comparison to Taxotere microtubule data (*dots*). To facilitate comparison, incoherent scattering has been approximately subtracted from the data (points) from *panel A* by passing a polynomial through the expected zeros of a microtubule scattering pattern. The substructure of the microtubule wall was modeled first, as indicated by the *inset*. At these angles the model fitting is practically independent of the number of protofilaments ($12 \leq n \leq 14$) and of subtracting or not subtracting the incoherent scattering from the data. The non-globular tubulin monomer employed is the same as that previously used to model Taxol-induced microtubules and consists of a set of 21 solid spheres of diameter 1.2 nm within a roughly triaxal ellipsoidal envelope of axes ~4 × 7 × 8 nm (37, 38). The monomers were placed in a three-start *n*-protofilament 18-monomer-long helical microtubule lattice (pitch 12.3 nm), and their orientation and lateral spacing were systematically varied. The best fit was obtained for the same orientation and at a lateral spacing of 5.7 nm, as shown by *solid curve 2* (*inset*). The *dashed* and *thin-line curves 2* correspond to similarly constructed four-start (pitch 16.4 nm) and two-start (pitch 8.2 nm) lattices, respectively. *Curves 1* and *3* (*inset*) are three-start models in which the lateral spacing is 5.9 and 5.5 nm, respectively. When a non-optimized tubulin monomer shape derived from the dimer solution scattering pattern (37) was directly employed, essentially the same 5.7 ± 0.1-nm fit to the J_n peak was obtained. The three-start microtubule models with a 5.7-nm lateral spacing were modified to contain 12 (diameter 21.8 nm), 13 (diameter 23.6 nm), or 14 protofilaments (diameter 25.4 nm), with the resulting changes in the position of their J_0 maxima. The effect of changing the microtubule wall thickness without modifying the microtubule mean diameter was also computed, comparing otherwise identical microtubules with 10% thicker or 10% thinner wall (not shown). This procedure gives an approximately similar change of mass of the microtubule as adding or taking out one protofilament, and it changes the intensities but not the positions of the scattering maxima, which is in contrast to the effect observed in *panel A* and is not compatible with the Taxotere and Taxol microtubule data.

constructed. Their resulting model scattering intensity profiles, which differ in the position and intensities of the J_0 peaks and are essentially identical at higher angles, are shown in Fig. 3*C*. Only the 13- and 14-protofilament microtubule models approach the experimental positions of the J_0 peaks in the Taxotere microtubule data. Actually, interpolating between the corresponding J_0 positions suggests that the Taxotere-induced microtubules would have 13.4 protofilaments, which indicates that its population is really a mixture of microtubules with different protofilament numbers. This same modeling procedure applied to the Taxol-induced microtubules (not shown) indicated 12.1 protofilaments. There is a limitation to this modeling; if incoherent scattering is not subtracted from the taxoid-induced microtubule data (compare uncorrected and corrected data in Fig. 3, *A* and *C*, respectively) the scattering at higher angle is not substantially modified, but the valley and peak intensities of the experimental J_0 peaks cannot be model-fitted by cylindrically closed microtubule structures. This is due to the mixture of different protofilament numbers and also suggests the presence in the solution of other strongly scattering polymers with similar substructure, possibly opened microtubules. Therefore such modeling procedure is useful to explore the main features of the microtubule wall in solution, although it is clearly an oversimplification due to the heterogeneity of the polymers formed at lower resolution.

Fig. 4 shows the distributions of protofilament numbers in electron micrographs of tannic acid-stained thin transverse sections of Taxotere- and Taxol-induced microtubules. The modal values are 13 and 12 protofilaments/microtubule, respectively. The average values are 13.4 and 12.2 protofilaments, which is fully consistent with the average diameter ratio determined by x-ray scattering and with the model-interpolated protofilament numbers. Opened tubular structures were also observed. On the other hand, along lateral views of undistorted microtubules, fringe patterns can be observed, which are generated by superposition of the images of the protofilaments in the front and back and depend on the twist of the lattice. The type of pattern and its repetition period permit determination of the number of protofilaments by direct comparison with microtubule model projections (37, 41, 42). Fig. 5 (*panels 1–3*) show typical lateral views of negatively stained Taxotere-induced microtubules assembled from GDP-tubulin, with the characteristic fringe patterns which are consistent with 12-, 13-, and 14-protofilament three-start microtubule lattices, respectively, saving potential distortions due to flattening onto the grid (37). Transitions between these different fringe patterns were also observed along the same microtubule (not shown). *Panel 4* in Fig. 5 shows a Taxotere-induced microtubule opening up on a background of curved tubulin oligomers. Tubulin double rings (not shown) could also be observed.

Finally, when model microtubule populations are simulated employing the protofilament distribution determined by electron microscopy, computed direct scattering curves are obtained (Fig. 2, *tracings 3* and *6*; Table I), which fit the experimental peak positions and approach their uncorrected relative intensities (Fig. 2, *tracings 1, 2, 4,* and *5*), thus modeling the mixture of different protofilament numbers in the assembled tubulin solution. Note that if pure cylindrically closed microtubules of a single protofilament number were employed, the computed scattering profiles would have considerably deeper minima (not shown), which becomes inconsistent with the data.

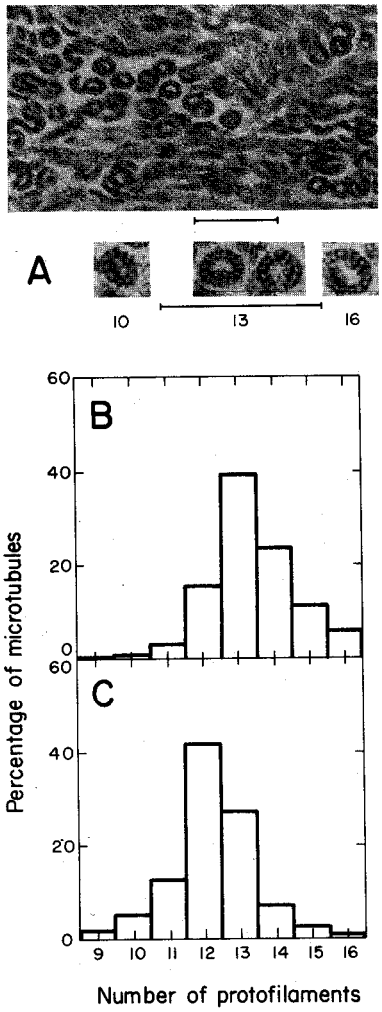

FIG. 4. *Panel A*, characteristic electron micrographs of transversely sectioned Taxotere microtubules, obtained from tannic acid-stained specimens prepared as reported (48). *Panel B*, distribution of protofilament numbers in tubulin-Taxotere microtubules. *Panel C*, same in tubulin-Taxol microtubules.

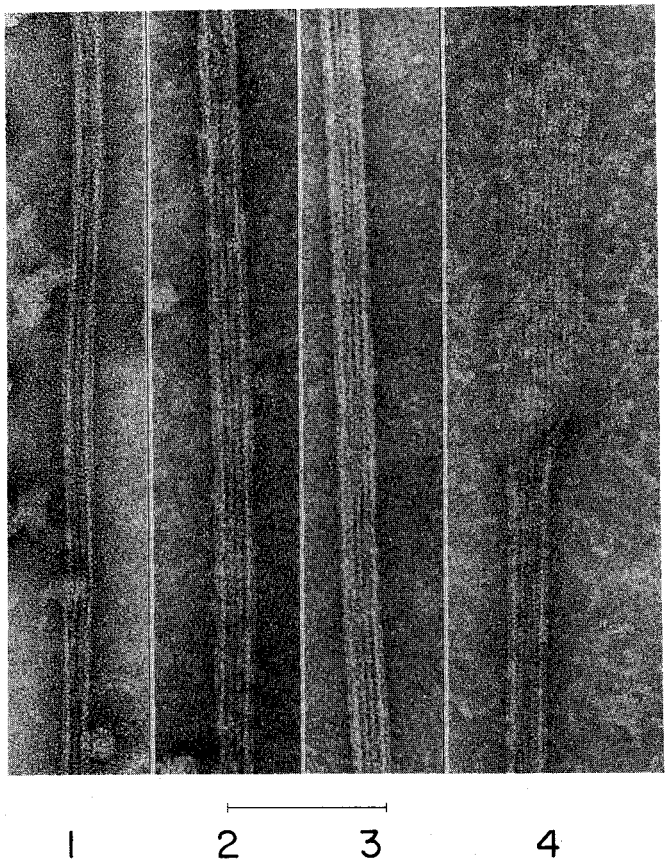

FIG. 5. **Lateral electron microscope projections of single Taxotere-induced microtubules in negative stain.** The *bar* corresponds to 100 nm. The white fringe patterns observed along each microtubule can be compared to model microtubule mass projections (see Fig. 7 in Ref. 37). Microtubule 1 shows a two-fringe/blur/one-fringe pattern and period consistent with a 12-protofilament three-start lattice. Microtubule 2 shows two longitudinal fringes, slightly off-side, corresponding to the 13-protofilament three-start lattice. Microtubule 3 shows an alternating two-fringe/three-fringe pattern, corresponding to a 14-protofilament three-start lattice. Microtubule types 2 and 3 were observed more frequently than type 1. In this experiment the assembly of 10 μM GDP-tubulin in PEDTA buffer (10 mM phosphate, 1 mM EDTA) containing 1 mM GDP and 10 μM taxotere at 37 °C was initiated by addition of 8 mM $MgCl_2$ (final pH 6.7), and after 90 min, the samples were adsorbed to Formvar- and carbon-coated grids, negatively stained with 2% uranyl acetate and photographed with a Philips EM420 electron microscope. Other conditions of assembly with Taxotere, such as addition of the drug to GTP-tubulin in $MgCl_2$-containing buffer in the cold, and initiation of assembly by a temperature shift to 37 °C resulted in similar observations.

DISCUSSION

Low Resolution Solution Structure of Microtubules Induced by Taxotere—The x-ray solution scattering of Taxotere-induced microtubules conforms to the known surface lattice of microtubules (39) with non-globular tubulin monomers. The substructure of the wall of microtubules can be modeled directly from the solution scattering and the helical monomer surface lattice. While the resulting microtubule model cannot be demonstrated to be unique, it describes the solution structure of microtubules to 3-nm resolution. Some of its features are common with electron microscopy and fiber diffraction models (39, 43, 44). The Taxotere-induced microtubule model (Fig. 3*C*) is very similar to a previous model of Taxol-induced microtubules (see Figs. 5*C* and 11 in Ref. 37), but with 13 instead of 12 protofilaments. This is representative of the majority of the Taxotere-induced microtubules in this study and of the typical number of protofilaments in cellular microtubules (45), although microtubules with other protofilament numbers are known (46, 47). *In vitro* assembled microtubules are well known to consist of a mixture of protofilament numbers that depends on solution conditions (42, 48). Taxotere-induced microtubules also have a distribution of different protofilament numbers, as shown by electron microscopy and by fitting their corrected x-ray scattering profiles. Modeling mixtures of different protofilament numbers has permitted fit of the positions and approximate intensities of the different maxima of the uncorrected scattering profiles of the assembled tubulin solutions. The similarity of Taxotere to control microtubules assembled with glycerol or associated proteins (this work and Ref. 37) suggests non-significant perturbation induced by this ligand, in marked contrast with the case of the majority of 12-protofilament in Taxol-induced microtubules. While the ability to change the number of protofilaments is a property of microtubule assembly, the differences observed are clearly induced by the taxoids binding under otherwise identical solution conditions. The predominant 12-protofilament lattice of Taxol-induced microtubules should simplify x-ray fiber diffraction analysis of the structure of microtubules, because the phases for the equatorial maxima are either 0 or π (since the projection on the basal plane of the microtubule, *i.e.* the transform of the equator, is centrosymmetric). On the other hand, the better solubility, microtubule assembly-inducing activity (31, 32), and availability of Taxotere leads us to prefer this ligand to experimentally stabilize microtubules, monitored by appropriate electron microscopy controls (37, 41, 42).

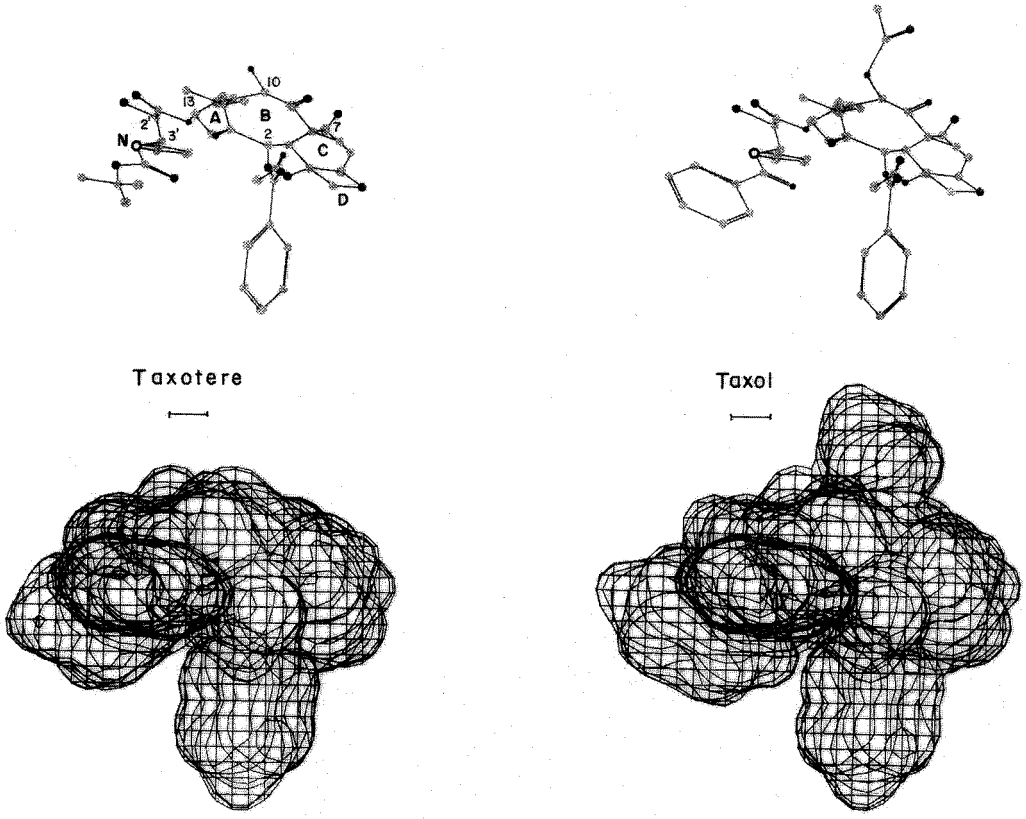

FIG. 6. **Molecular models of Taxotere and Taxol.** Shown in the *upper part* are stick models (hydrogen atoms have not been drawn), and in the *lower part* the corresponding Van der Waals contour projections including the hydrogen atoms. Note the excess volume of the Taxol side chain and acetyl substituent. The *bar* corresponds to 0.1 nm. Models were constructed employing the crystallographic atomic coordinates of Taxotere (58) with the program Chem-X. Due to the congested nature of these compounds (6), models should be examined together with the chemical structures. The phenyl group at position 3′ is at the back and perpendicular to the plane in this projection.

Effects of the Binding of the Taxol Side Chain on Microtubule Structure—Induction of tubulin assembly with Taxol instead of Taxotere results in apparently identical microtubule wall substructure but changes the more frequent lateral bonding angle between tubulin molecules from 152.3° to 150°, *i.e.* from the 13- to the 12-protofilament microtubule forming geometry respectively. Which changes in the binding of ligand to tubulin are responsible for the change of the assembled protein structure? Views of the three-dimensional structures of Taxotere (*N-tert*-butoxycarbonyl-10-deacetyl-*N*-debenzoyl Taxol) and Taxol are compared in Fig. 6. Two large parts can be clearly distinguished in these molecules, the taxane ring system (consisting of rings A, B, C, and D) and the side chain at C-13. Among several modifications of the taxane ring system, opening of the oxiethane ring D or deletion of the *O*-benzoyl group in position 2 drastically reduce activity. However, deacetylation at C-10 or substitution of the hydroxyl at position C-7 (top part of the molecules), are known to cause insignificant changes (4–6). The side chain (with a free hydroxyl group at position 2′ and a phenyl group at 3′) is essential for taxane activity, which is reduced more than 1000-fold in baccatin III (4, 5). The side chain modification in Taxotere consists in substitution of an *N-tert*-butoxycarbonyl in place of the *N*-benzoyl group of Taxol. This changes the Van der Waals contour of the molecule by a few tenths of a nanometer in that region (see Fig. 6) and causes very minor modification of the computed charge distribution (not shown). This strongly suggests, assuming little effect of the deacetylation at C-10, that the change observed in the protofilament number between Taxotere- and Taxol-induced microtubules is linked to the binding of the side chain of Taxol to microtubules.

Gueritte-Voegelein *et al.* (19) have proposed that the taxane skeleton (which is active on *Physarum* tubulin) binds to its site on microtubules, the binding being stabilized by a specific interaction of the attached side chain, which is inactive by itself (19). In this sense the taxol-tubulin binding might resemble the interactions with tubulin of other bidentate ligands, such as colchicine (49) and *Vinca* alkaloids (50), in which the binding of the two covalently linked ligand moieties to its specific subsite is entropically favored over the independent binding of the two separate parts (51). Swindell *et al.* (20) have proposed that the Taxol recognition site on microtubules possesses a hydrophobic cleft that accepts a side chain having the appropriate stereochemistry and hydrogen bonding, which is exemplified by the Taxotere side chain. Among several possible explanations to the change in protofilament number, we currently favor the simple hypothesis that the taxoids would more likely bind to microtubules between protofilaments (30) and modify their lateral contact angle. This is fully compatible with the independent thermodynamically based proposal that taxoids may constitute double-sided ligands, which bind to tubulin at the microtubule end and participate in a contact interface with the newly added tubulin molecule, thus stabilizing the assembly, while allosteric mechanisms cannot be excluded (32). Analysis of the time-resolved x-ray scattering data during taxoid-induced assembly is compatible with the notion that these ligands induce the lateral accretion of protofilaments.[2] The location of the taxoid binding site on the three-dimensional structure of microtubules could be approached by x-ray scattering employing heavy atom-labeled derivatives.

[2] J. F. Díaz, J. M. Andreu, G. Diakun, and J. Bordas, unpublished data.

Microtubule Lattice Defects, Opening by Taxotere Excess, and Taxoid-induced Microtubule Flexibility—It is known that the number of protofilaments can change along individual microtubules, implying defects in their surface lattice (48), and that assembled microtubules can associate end to end (52, 53). The optimal proportion of one Taxotere molecule per tubulin dimer for microtubule assembly, as determined by x-ray scattering in this study, is in full agreement with the biochemical properties of the system (31). However, cylindrical features diminish in ligand excess (Fig. 1). A similar effect had been preliminarily observed with Taxol (37). The simplest interpretation is that microtubules in taxoid excess open with respect to those in unitary ligand to tubulin ratio. Consider the taxoid binding site hypothetically constituted by two half-sites in adjacent tubulin molecules (see above and Fig. 9 in Ref. 32). In excess ligand it is possible that two different taxoid molecules occupy the two half-sites at equilibrium, causing the dissociation of the adjacent tubulin molecules. Having a small percentage of tubulin molecules doubly liganded in one microtubule would induce bonding mismatches in the microtubule lattice. Such a defect could be propagated through the lattice or localized at a seam closing the microtubule (37, 54). The latter would be enough to locally open microtubules.

Microtubules are relatively rigid cylindrical structures. Although Taxol was initially reported to increase microtubule rigidity (55), it has now been shown that the flexibility of individual assembled microtubules increases immediately by effect of Taxol (56, 57). In contrast with the exchangeable nucleotide, which becomes non-dissociable in assembled tubulin, Taxol, and Taxotere appear rapidly interchangeable in microtubules,[3] indicating that the taxoid binding site is very accessible. Dye *et al.* (56) have proposed that taxol modifies the interactions between protofilaments, allowing them to slip relative to each other. How can this be reconciled with the fact that taxoid binding stabilizes microtubules and with the proposal that these ligands bridge adjacent protofilaments? Taxoid-induced microtubule thermodynamic stability is linked to the binding of the ligand (32) and is compatible with the polymer structure being more flexible. Given a lateral spacing of 5.7 nm, the maximal curvature measured (radius about 15 μm; Ref. 56) corresponds to a displacement of adjacent protofilaments relative to each other of about the length of 1 in 3300 tubulin monomers. Such an effect, if continuous, would bring many laterally adjacent tubulin molecules out of register along the microtubule. Discrete slipping of adjacent protofilaments by one monomer along the whole microtubule length seems feasible, since the lateral contacts between α and β monomers are believed to be largely equivalent (37). Alternately, a low frequency of discrete defects (empty positions) spread through the microtubule lattice might decrease the shear resistance of the walls. Clearly, local opening of the microtubules may also facilitate bending. Both later effects might be related to a small fraction tubulin molecules doubly liganded to taxoid. On the other hand, Venier *et al.* (57) have indicated that Taxol and Taxotere affect the superstructure of microtubules, apparently inducing a helicoidal shape of pitch ≈15 μm. If this bending were related to a change in protofilament number, it would be periodic (going from 13 to 12 or 14 protofilaments by lattice tilting can be calculated to generate respectively a right- or left-handed protofilament twist of period ≈4 μm; Ref. 37 and present work), and it would change among different microtubules in the population, even in taxoid-less microtubules. Otherwise the bending should be due to the taxoid binding itself.

Acknowledgments—We thank the staff of Daresbury Laboratory, Dr. E. Pantos for the scattering simulation program DALAI, and Dr. Greg Diakun for extensive help during measurements. We thank Dr. M. Menendez, Instituto de Quimica Fisica del CSIC, for helpful discussion, Dr. J.-L. Fabre, Rhône-Poulenc Rorer, for Taxotere and Dr. M. Suffness, NCI, National Institutes of Health, for Taxol. We acknowledge the expert help of M. A. Ollacarizqueta and D. Guirao with electron microscopy and A. Hurtado for drawings.

[3] J. F. Díaz and J. M. Andreu, unpublished data.

REFERENCES

1. Wilson, L., and Jordan, M. A. (1994) in *Microtubules* (Hyams, J. S., and Lloyd, C. W., eds) pp. 59–83, Wiley-Liss, New York
2. Briand, C., Barra, Y., Manfait, M., Timasheff, S. N., Tew, K. D., and Tapiero, H. (eds) (1993) *Cell. Pharmacol.* **1,** Suppl. 1, S1–S121
3. Wani, M. C., Taylor, H. L., Wall, M. E., Coggon, P., and McPhail, A. T. (1971) *J. Am. Chem. Soc.* **93,** 2325–2327
4. Kingston, D. G. I. (1991) *Pharmacol. Ther.* **52,** 1–34
5. Guenard, D., Gueritte-Voegelein, F., and Potier, P. (1993) *Acc. Chem. Res.* **26,** 160–167
6. Nicolaou, K. C., Dai, W. M., and Guy, R. K. (1994) *Angew. Chem. Int. Ed. Engl.* **33,** 15–44
7. Rowinsky, E. K., Cazenave, L. A., and Donehower, R. C. (1990) *J. Natl. Cancer Inst.* **82,** 1247–1259
8. Donehower, R. C., and Rowinsky E. C. (1993) *Cancer Treat. Rev.* **19,** Suppl. C, 63–78
9. Schiff, P. B., Fant, J., and Horwitz, S. B. (1979) *Nature* **277,** 665–667
10. Schiff, P. B., and Horwitz, S. B. (1980) *Proc. Natl. Acad. Sci. U. S. A.* **77,** 1561–1565
11. Horwitz, S. B. (1992) *Trends Pharmacol. Sci.* **13,** 134–136
12. Jordan, M. A., Toso, R. J., Thrower, H., and Wilson, L. (1993) *Proc. Natl. Acad. Sci. U. S. A.* **90,** 9552–9556
13. Fett-Neto, A. G., DiCosmo, F., Reynolds, W. F., and Sakata. K. (1992) *Bio/Technology* **10,** 1572–1575
14. Stierle, A., Strobel, G., and Stierle, D. (1993) *Science* **260,** 214–216
15. Nicolaou, K. C., Yang, Z., Liu, J. J., Ueno, H., Nanternet, P. G., Guy, R. K., Clairborne, C. F., Renaud, J., Couladouros, E. A., Paulvannan, K., and Sorensen, E. J. (1994) *Nature* **367,** 630–634
16. Holton, R. A., Somoza, C., Kim, H. B., Liang, F., Bieidger, R. J., Boatman, P. D., Shindo, M., Smith, C., Kim, S., Nadizadeh, H., Suzuki, Y., Tao, C., Vu, P., Tang, S., Zhang, P., Murthi, K. K., Gentile, L. N., and Liu, J. H. (1994) *J. Am. Chem. Soc.* **116,** 1597–1598; 1599–1600
17. Denis, J. N., Greene, A. E., Guénard, D., Gueritte-Voegelein, F., Mangatal, L., and Potier, P. (1988) *J. Am. Chem. Soc.* **110,** 5917–5919
18. Mangatal, L., Adeline, M. T., Guénard, D., Gueritte-Voegelein, F., and Potier, P. (1989) *Tetrahedron* **45,** 4177–4190
19. Gueritte-Voegelein, F., Guénard, D., Lavelle, F., LeGoff, M. T., Mangatal, L., and Potier, P. (1991) *J. Med. Chem.* **34,** 992–998
20. Swindell, C. S., Krauss, N. E., Horwitz, S. B., and Ringel, I. (1991) *J. Med. Chem.* **34,** 1176–1184
21. Ringel, I., and Horwitz, S. B. (1991) *J. Natl. Cancer Inst.* **83,** 288–291
22. Barasoain, I., de Inés, C., Díaz, J. F., Andreu, J. M., Peyrot, V., Leynadier, D., Garcia, P., and Briand, C. (1991) *Proceeding of the American Association for Cancer Research* **32,** 329
23. Bissery, M. C., Guenard, D., Gueritte-Voegelein, F and Lavelle, F. (1991) *Cancer Res.* **51,** 4845–4852
24. Riou, J. F., Naudin, A., and Lavelle, F. (1992) *Biochem. Biophys. Res. Commun.* **187,** 164–170
25. Maurer, H. R., Eckert, K., and Bissery, M. C. (1993) *Int. J. Oncol.* **3,** 161–165
26. Tomiak, E., Piccart, M. J., Kerger, J., Devaleriola, D., Tueni, E., Lossignol, D., Lips, S., Le Bail, N., and Bayssas, N. M. G. (1991) *Eur. J. Cancer* **27,** 1184–1991
27. Pazdur, R., Newman, R. A., Newman, B. M., Fuentes, A., Benvenuto, J., Bready, B., Moore, D., Jr., Jaiyesimi, I., Vreeland, F., Bayssas, M. M. G., and Raber, M. N. (1992) *J. Natl. Cancer Inst.* **84,** 1781–1788
28. Rao, S., Krauss, N. E., Heerding, J. M., Swindell, C. S., Ringel, I., Orr, G. A., and Horwitz, S. B. (1994) *J. Biol. Chem.* **269,** 3132–3134
29. Combeau, C., Commercon, A., Mioskowski, C., Rousseau, B., Aubert, F., and Goeldner, M. (1994) *Biochemistry* **33,** 6676–6683
30. Howard, W. D., and Timasheff, S. N. (1988) *J. Biol. Chem.* **263,** 1342–1346
31. Díaz, J. F., and Andreu, J. M. (1993) *Biochemistry* **32,** 2747–2755
32. Díaz, J. F., Menendez, M., and Andreu, J. M. (1993) *Biochemistry* **32,** 10067–10077
33. Mandelkow, E. M., Harmsen, A., Mandelkow, E., and Bordas, J. (1980) *Nature* **287,** 595–599
34. Bordas, J., Mandelkow, E. M., and Mandelkow, E. (1983) *J. Mol. Biol.* **164,** 89–135
35. Andreu, J. M., García de Ancos, J., Starling, D. Hodgkinson, J. L., and Bordas, J. (1989) *Biochemistry* **28,** 4036–4040
36. Lattman, E. E. (1994) *Curr. Opin. Struct. Biol.* **4,** 87–92
37. Andreu, J. M., Bordas, J., Díaz J. F., García de Ancos J., Gil R., Medrano, F. J., Nogales E., Pantos, E., and Towns-Andrews, E. (1992) *J. Mol. Biol.* **226,** 169–184
38. Díaz, J. F., Pantos, E., Bordas, J., and Andreu, J. M. (1994) *J. Mol. Biol.* **238,** 214–225
39. Amos, L. A., and Klug, A. (1974) *J. Cell Sci.* **14,** 523–549
40. Pantos, E., and Bordas, J. (1994) *J. Pure Appl. Chem.* **66,** 77–82
41. Wade, R. H., Chrétien, D., and Job, D. (1990) *J. Mol. Biol.* **212,** 775–786
42. Ray, S., Meyhöfer, E., Milligan, R. A., and Howard, J. (1993) *J. Cell Biol.* **121,** 1083–1093
43. Mandelkow, E., Thomas, J., and Cohen, C. (1977) *Proc. Natl. Acad. Sci. U. S. A.* **74,** 3370–3374
44. Beese, L. Stubbs, G., and Cohen C. (1987) *J. Mol. Biol.* **194,** 257–264

45. Tilney, L. G., Brian, J., Bush, D. J., Fujiwara, K., Mooseker, M. S., Murphy, D. B., and Snyder, D. H. (1973) *J. Cell Biol.* **59,** 267–275
46. Chalfie, M., and Thomson, J. N. (1982) *J. Cell Biol.* **93,** 15–23
47. Dallai, R., Afzelius, B. A., Lanzavecchia, S., and Bellon, P. L. (1993) *Cell Motil. Cytoskel.* **24,** 49–53
48. Chrétien, D., Metoz, F., Verde, F., Karsenti, E., and Wade, R. H. (1992) *J. Cell Biol.* **117,** 1031–1040
49. Andreu, J. M., and Timasheff, S. N. (1982) *Biochemistry* **21,** 534–543
50. Prakash, V., and Timasheff, S. N. (1991) *Biochemistry* **30,** 873–880
51. Timasheff, S. N., Andreu, J. M., Gorbunoff, M. J., Medrano, F., and Prakash, V. (1993) *Cell. Pharmacol.* **1,** Suppl. 1, S27–S33
52. Rothwell, S. W., Grasser, W. A., and Murphy, D. B. (1986) *J. Cell Biol.* **102,** 619–627
53. Williams, R. C., Jr., and Rone, L. A. (1989) *J. Biol. Chem.* **264,** 1663–1670
54. Y. H. Song and Mandelkow, E. (1993) *Proc. Natl. Acad. Sci. U. S. A.* **90,** 1671–1675
55. Gittes, F., Mickey, B., Nettleton, J., and Howard, J. (1993) *J. Cell Biol.* **120,** 923–934
56. Dye, R. B., Fink, S. P., and Williams, R. C., Jr. (1993) *J. Biol. Chem.* **268,** 6847–6850
57. Venier, P., Maggs, A. C., Carlier, M. F., and Pantaloni, D. (1994) *J. Biol. Chem.* **269,** 13353–13360
58. Gueritte-Voegelein, F., Guenard, D., Mangatal, L., Potier, P., Guilhem, J., Cesario, M., and Pascard, C. (1990) *Acta Crystallogr. Sec. C* **46,** 784–788